MULTIFOCUS MOVEOUT REVISITED: DERIVATIONS AND ALTERNATIVE EXPRESSIONS

Martin Tygel, Lúcio T. Santos & Jörg Schleicher

DMA – IMECC – UNICAMP

Caixa Postal 6065

13081–970 Campinas (SP), Brazil

Abstract

The multifocus moveout of Gelchinsky and coworkers is a powerful tool for stacking multi-coveraged data in arbitrary configurations. Based on general ray theoretical assumptions and on attractively simple geometrical considerations, the multifocus moveout is designed to express the traveltimes of neighboring rays arbitrarily located around a fixed central, primary reflected or even diffracted, ray. In this work, the basic derivations and results concerning the multifocus approach are reviewed. A higher-order multifocus moveout expression that generalizes the corresponding one of Gelchinsky is obtained from slight modifications of the original derivation. An alternative form of the obtained multifocus expression that is best suited for numerical implementation is also provided. By means of a simple numerical experiment, we also coment on the accuracy of the multifocus traveltime approximations.

Introduction

Accurate and reliable traveltime moveout expressions are of prime importance in seismic processing and imaging because of their use in producing stacked sections. The most famous moveout expression is the normal and dip moveout (NMO/DMO) designed to describe the traveltime of primary reflections of common-midpoint (CMP) data. In many seismically relevant situations, the NMO/DMO process has been able to produce stacked sections with significant reduction of noise, also attenuating multiples and other undesirable events. Although CMP stacking under NMO/DMO

is a routine step in practically all seismic processing sequences in the oil industry, also a number of shortcomings of the method have been recognized. Being designed for gently dipping reflectors and small lateral velocity variations in the overburden, and moreover, for not too large offsets, the NMO/DMO moveout expression is no longer accurate when these conditions are severely violated. A second shortcoming is its dependence on the CMP configuration. In modern acquisition surveys, CMP data often represent only a fraction of the acquired data. As a consequence, moveout expressions that use arbitrary locations of source and receiver pairs around a fixed central point (that may even be a CMP point) are able to make a much better use of the available date and to profit from the significantly greater redundancy that is offered.

Several traveltime moveout formulas already exist in the literature that describe traveltimes along neighboring rays of a fixed central zero-offset (or normal) ray, with arbitrary locations of the source and receiver around the central point. These are the classical *parabolic/hyperbolic* moveouts (see, e.g., Ursin, 1982; Červený, 1985; Schleicher et al., 1993), the *optical stack* moveout of de Bazélaire (1988), the *multifocus* moveout of Gelchinsky (1988) and the recent *common reflection surface (CRS)* moveout of Höcht (1998). All the above traveltime moveout formulas are coincident in the second-order approximation of source and receiver offsets. An actual and objective comparison between them is not an easy task and remains a challenging problem. With the exception of the classical hyperbolic and parabolic moveouts, all the other formulas are, up to now, two-dimensional, which means that sources and receivers are located on a single seismic line and the medium does not vary in the out-of-plane direction.

The common goal of all these traveltime formulas is to provide stacking surfaces along which the multicoverage data can be optimally stacked in order to obtain the best possible simulated zero-offset section. Like in a standard velocity analysis by NMO stack, the parameters defining the traveltime surface allow for inversion for the medium velocity that may now, however, vary laterally.

In this note, we concentrate on the geometrically appealling multifocus moveout of Gelchinsky and coworkers. We feel it has not attracted the attention it deserves in the seismic literature and, perhaps, a great deal of its potential has not yet been sufficiently exploited. By reviewing the multifocus original derivations and results, as provided in several publications since the first presentation of Gelchinsky (1988) and summarized in Gelchinsky et al. (1997), we introduce a new expression of Gelchinsky's multifocus parameter that is not only slightly more general but also

implementationally more stable. Substitution into the original multifocus moveout formula leads to a higher-order approximation expression in terms of source and receiver offsets. The new parameter reduces to its previous counterpart by natural approximations. As a second contribution of the present analysis, we introduce a modification in the definition of Gelchinsky's asymmetry parameter, so as to have it dimensionless. Moreover, working with the reciprocal of the multifocus parameter leads to an alternative, mathematically equivalent moveout formula, which is more amenable for numerical implementation. By means of a simple illustrative numerical experiment, we comment on the performance of the multifocus traveltime formulas.

Gelchinsky's multifocus moveout

We assume that the subsurface can be described by a 2-D laterally inhomogeneous isotropic layered earth model. In this model, we further assume that the kinematics of body waves is well described by zero-order ray theory (see, e.g., Červený, 1985). We use Cartesian coordinates (x, z) and suppose that a dense multi-coverage seismic experiment has been carried out on a single seismic line along the x-axis. This implies that each point on the seismic line is surrounded by a set of shot-receiver pairs (within a certain range of offsets). The discreteness of real-world data may require trace interpolation to replace missing traces.

Referring to Figure 1, we consider a fixed target reflector Σ in depth, as well as a fixed *central* point X_0 on the seismic line, considered to be the location of a coincident source-receiver pair $S_0 = G_0 = X_0$. Also shown in Figure 1 is the two-way zero-offset reflection ray, called from now on the *central ray*. It hits the reflector at point R_0, known as the normal-incident-point (NIP). Figure 1 finally shows a pair of source and receiver points (S, G) together with its corresponding primary reflected ray SRG, relative to the target reflector Σ. The source and receiver pair (S, G) will be considered a generic description of all source-receiver pairs in the vicinity of the central point. We note incidently that the central ray, as well as the reflection ray SRG focus at point P in depth. This fact will be of importance later on. We use the horizontal coordinates x_0, x_S and x_G to specify the location of the central point X_0, the source S and the receiver G, respectively. The relative distances from a given source-receiver pair (S, G) to the fixed central point X_0,

$$\Delta x_S = x_S - x_0 \quad \text{and} \quad \Delta x_G = x_G - x_0 \ , \tag{1}$$

are called the source and receiver offsets, respectively.

Referring again to Figure 1, it is our aim to find an approximation of the traveltime of the reflection ray SRG in the vicinity of the central, zero-offset reflection ray $X_0R_0X_0$. We assume that the traveltime of the latter, as well as the medium velocity at the central point are given by the quantities T_0 and v_0, respectively. Suppose, as depicted in Figure 1, that the two rays SRG and $X_0R_0X_0$ cross at the unknown point P. Without loss of generality, we assume P to be on the source ray segment SR. The multifocus approach makes use of a hypothetical wave that originates at point P. This hypothetical wave is depicted in Figure 1 by two of its wavefronts. One, denoted by Σ_S, contains X_0 and has traveled up from P to the source point S. The other, denoted by Σ_G, also contains X_0 and has traveled from P down to the reflector Σ and from there towards the receiver point G. We denote the curvatures of these two wavefronts by K_S and K_G, respectively. Note that a true wave originating at S with an initial curvature of $-K_S$ focuses at P and emerges at G with curvature K_G. We will refer to this wave as the *focusing wave*.

By construction, the traveltime of the focusing wave from the wavefront Σ_S to the wavefront Σ_G, is the given zero-offset traveltime T_0. As a consequence, we can express the traveltime for the ray SRG in the form

$$\mathcal{T} = T_0 + \Delta T_S + \Delta T_G \ , \tag{2}$$

where ΔT_S and ΔT_G are the *multifocus* source and receiver moveouts. Let the medium velocity in the vicinity of the central point X_0 be constant and denoted by v_0. Under the assumption that the wavefronts Σ_S and Σ_G can be approximated by circles with radii $R_S = 1/K_S$ and $R_G = 1/K_G$ and centers C_S and C_G, respectively, it can be shown by simple geometrical considerations that the above multifocus moveouts can be determined. In Figure 2, the situation is explained at the source point S. An analogous construction is valid at the receiver point G. The multifocus moveout ΔT_S is the traveltime from S to S', assuming the segment SS' to be a straight line. Within the triangle $S\widehat{C_S}X_0$ we have by the law of cosines that

$$\overline{SC_S}^2 = \overline{SX_0}^2 + \overline{C_SX_0}^2 - 2\overline{SX_0}\,\overline{C_SX_0}\cos(\frac{\pi}{2} + \beta_0) \ , \tag{3}$$

where β_0 denotes the emergence angle of the central ray. The sign of β_0 is defined as negative when the central ray impinges from the right as in Figure 2. Identifying $\overline{SX_0} = \Delta x_S$, $\overline{C_SS'} = \overline{C_SX_0} = R_S = 1/K_S$, and $\overline{SC_S} = R_S + \overline{SS'}$, solving equation (3) for $\overline{SS'}$, and dividing by v_0, we arrive at

$$\Delta T_S = \frac{1}{v_0\,K_S}\left[\sqrt{1 + 2K_S\,\sin\beta_0\,\Delta x_S + (K_S\,\Delta x_S)^2} - 1\right] \ , \tag{4}$$

where we have chosen the sign of the square root according to the physical condition that ΔT_S has to be positive for positive curvature K_S. The same formula with all indices S changed to G holds for ΔT_G.

The two fundamental eigenwaves

As shown by Gelchinsky et al. (1997) using basic dynamic ray tracing arguments (see Appendix), the curvatures $K_S = 1/R_S$ and $K_G = 1/R_G$ of the down- and upgoing wavefronts of the hypothetical focusing wave satisfy the relationships

$$K_S = \frac{K_{NIP} - \Gamma K_N}{1 - \Gamma} \quad \text{and} \quad K_G = \frac{K_{NIP} + \Gamma K_N}{1 + \Gamma} \; . \tag{5}$$

In the above formula, K_N and K_{NIP} are the curvatures of the classical *normal* (N) wave and the *normal-incidence-point* (NIP) wave introduced by Hubral (1983) in connection with true-amplitude migration. Moreover, Γ is a modified version of the *focusing parameter* of Gelchinsky et al. (1997). It is defined as the reciprocal of the original focusing parameter γ introduced by Gelchinsky, i.e., $\Gamma = 1/\gamma$. The mentioned N and NIP waves are two hypothetical waves defined as follows: (a) The N wave starts as a wavefront that coincides with the target reflector Σ, propagates upwards with half the medium velocity and arrives at the central point X_0 at time T_0. (b) The NIP wave starts at the target reflector Σ as a point source at the NIP point R_0, propagates upwards with half the medium velocity and arrives at the central point X_0 also at time T_0. As is well known (Hubral, 1983) both these waves are *eigenwaves* in the following sense: If their wavefronts propagate downwards, reflect at Σ and propagate upwards to the surface, their arriving wavefronts at the central point X_0 coincide with their corresponding initial wavefronts. Moreover, the relative geometrical-spreading factors of the N and NIP waves are plus or minus unity at X_0, respectively.

The modified focusing parameter Γ controls the location along the central ray (or along its continuation) of the focusing point P which is determined by the central ray and the neighboring reflecting ray SRG. In other words, for neighboring reflecting rays, we have a one-to-one correspondence between the value of the focusing parameter and the location of the focusing point. This is the reason why the present approximation formulas are called multifocus. Let us see how this relates to the N and NIP waves introduced above. Up to second-order approximation of the traveltime with respect to the source and receiver offsets, the N wave can be considered as a wave focusing at the center of curvature of the reflector, because neighboring rays to the central ray are also normal

rays. This wave is described by setting the focusing parameter $\Gamma = \Gamma_N = \infty$. Substitution into equation (5) yields $K_S = K_G = K_N$ as expected. In the same approximation, the NIP wave can be considered as a wave focusing at the NIP point R_0. The focusing parameter for this wave is $\Gamma = \Gamma_{NIP} = 0$. We find from equation (5), $K_S = K_G = K_{NIP}$, as required. With the introduction of the modified focusing parameter Γ, the physical interpretation for the N and NIP waves are much more appealing. For instance, one can directly observe from the above that for positive Γ, the focus point P falls below the reflector – or, in other words, onto the upgoing ray segment RG – and for negative Γ, P is above the reflector or on the segment SR.

For the relationship between the multifocus parameter γ and any actual source and receiver offsets Δx_S and Δx_G, Gelchinsky et al. (1997) obtained the approximation [see their eq. (17), here corrected for a wrong sign and a factor 2]

$$\gamma = \frac{\Delta x_G - \Delta x_S}{\Delta x_G + \Delta x_S - K_{NIP} \sin\beta_0 \Delta x_G \Delta x_S} \ . \tag{6}$$

This formula is valid to second-order approximation in Δx_S and Δx_G. The corresponding first-order approximation is given by the simpler expression

$$\gamma = \gamma_0 = \frac{\Delta x_G - \Delta x_S}{\Delta x_G + \Delta x_S} \ . \tag{7}$$

The above formula has been also obtained by Tygel et al. (1997) by an independent method, but following the same multifocusing principles.

Alternative multifocus expressions

In this section, we introduce some alternative definitions and expressions that relate to the multifocus moveout. The main objective of the new formulas is to have them in a most accurate and useful form, especially for direct numerical implementation. The obtained results followed upon slight modifications of the derivations of the original multifocus expressions, as presented in Gelchisnky et al. (1997).

The modified focusing parameter

The alternative multifocus moveout expression to be presented below will be given in terms of the modified focusing parameter, $\Gamma = 1/\gamma$. As shown in the Appendix, we find for the modified focusing parameter the expression

$$\Gamma = \Gamma_0 + \frac{\mu}{2}\,(1 - \Gamma_0^2)\;, \tag{8}$$

where Γ_0 is the reciprocal of the zero-order approximation of the original multifocus parameter (see equation (7))

$$\Gamma_0 = \frac{1}{\gamma_0} = \frac{\Delta x_G + \Delta x_S}{\Delta x_G - \Delta x_S}\;. \tag{9}$$

Also, μ is given by

$$\mu = \Lambda\,(1 + \Lambda)\;, \tag{10}$$

where Λ is the *modified asymmetry parameter* given by

$$\Lambda = \frac{1}{2}(\Delta x_G - \Delta x_S)\,K_{NIP}\,\sin\beta_0\;. \tag{11}$$

The modified asymmetry parameter Λ defined above is nothing else than a dimensionless counterpart of the original asymmetry parameter $\alpha = K_{NIP}\sin\beta_0$ introduced by Gelchinsky (1988) in the description of the Common Reflection Element (CRE) Method. The asymmetry parameter plays a significant role in the selection of source-receiver pairs for which the corresponding reflection rays reflect on a single point. The modification of the asymmetry parameter deserves an explanation. In the derivation of the formula for the traveltime, we have to perform some Taylor expansions for small values of the asymmetry parameter. Therefore, it is necessary to have it dimensionless in order to have a well-defined meaning for "small".

Reduction to previous formulas.—We consider the approximation of the modified focusing parameter Γ when the modified asymmetry parameter Λ becomes small. Comparing formulas (7) and (6) with the new approximation (8), we readily recognize that the former ones are the zero-order ($\mu = 0$) and first-order ($\mu = \Lambda$) approximations, respectively, of the latter.

General multifocus formula

To present the multifocus traveltime expression suitable for numerical implementation, we start by rewriting formula (4) for the multifocus moveout ΔT_j as

$$\Delta T_j = \frac{\Delta x_j}{v_0\, k_j}\left[\sqrt{1+2k_j\,\sin\beta_0+k_j^2}-1\right], \quad j=S,G\,, \tag{12}$$

where we have introduced the *dimensioneless curvatures*

$$k_j = \Delta x_j K_j, \quad j=S,G\,. \tag{13}$$

The proposed alternative, mathematically equivalent multifocus traveltime expression (compare with equations (2) and (4)) is

$$\mathcal{T} = T_0 + \frac{1}{v_0}\left[M_S\Delta x_S + M_G\Delta x_G\right]\,, \tag{14}$$

where

$$M_j = \frac{k_j+2\sin\beta_0}{1+\sqrt{1+k_j(k_j+2\sin\beta_0)}}\,, \tag{15}$$

and

$$k_j = \frac{\Delta x_G-\Delta x_S}{2-\mu(\Gamma_0\pm 1)}[\Gamma K_N \mp K_{NIP}]\,. \tag{16}$$

Here, the upper sign holds for $j=S$ and the lower one for $j=G$. In zero-order approximation ($\Lambda=0$) the above expression (16) for k_j reduces to

$$k_j = \frac{(\Delta x_G+\Delta x_S)}{2}K_N \mp \frac{(\Delta x_G-\Delta x_S)}{2}K_{NIP}\,. \tag{17}$$

The motivation behind the above formulas is that in numerical computations dimensionless quantities and large positive denominators are welcome, in order to prevent for overflow or underflow problems. In particular, for $K_j \approx 0$ the above expression is more stable than the corresponding original multifocus formulas (2) to (4).

Numerical illustration

In this section, we evaluate the quality of the above traveltime approximations by means of a simple numerical example. As a first numerical test we study their behaviour for the simple earth model depicted in Figure 3. It consists of two acoustic homogeneous media separated by a smooth

interface. The velocities above the reflector is a constant v_0 =4 km/s. The reflector consists of a straight line on the left side, a circular element in the center, and an element with varying curvature on the right side. We consider three different central points at $X_0 = -1750$ m, 400 m, and 1650 m, indicated by vertical bars.

Figure 4a shows the true reflection traveltime surface in the vicinity of $X_0 = -1750$ m, together with its approximations by the above formulas, as a function of midpoint and half-offset. For reasons of comparison, we also include the *hyperbolic traveltime approximation* (Tygel et al., 1997), given by

$$\begin{aligned} \mathcal{T}^2 &= \left(\mathcal{T}_0 + \frac{\sin\beta_0}{v_0}(\Delta x_S + \Delta x_G)\right)^2 + \\ &\quad \frac{\mathcal{T}_0 \cos^2\beta_0}{2v_0}\left(K_N(\Delta x_S + \Delta x_G)^2 + K_{NIP}(\Delta x_G - \Delta x_S)^2\right) . \end{aligned} \tag{18}$$

Note that apart from the right-hand side of Figure 4a, all traveltime surfaces seem to coincide perfectly. Figure 4b shows the relative errors of the different approximations. Since it is hard to appreciate the results in Figure 4, we show two cross cuts through Figure 4b along the half-offset axis at midpoints -1750 m (marked by a cross), i.e., at the chosen central point, and at -1350 m (marked by an asterisk), i.e., 400 m to the right of the central point. These cross cuts are shown in the top left and top right graphs of Figure 5.

The hyperbolic traveltime formula (18) is exact for a planar dipping reflector, which leads to a zero error in the top left graph of Figure 5. Observe that in the top right graph the error deviates from zero for half-offsets larger than 600 m, because the reflection point is already on the circular part of the reflector. As expected, the second-order approximation is better than that of the first order. Interestingly enough, however, the multifocus traveltime formula (14) shows the best fit for zero order, i.e., for $\mu = 0$.

The corresponding cross plots for the central points $X_0 = 400$ m and $X_0 = 1650$ m are shown in the center and bottom parts of Figure 5, respectively. The left graph in each line shows the results in the CMP section at the respective central point, and the right graph shows those of the CMP section 400 m to the right, i.e., at 800 m and 2050 m, respectively. We recognize that on the circular part of the reflector the zero-order multifocus traveltime approximation yields the least error. On the most realistic part of the reflector, where the curvature varies, it is not possible to decide which approximation is the best. Their behaviour depends on the local properties of the

medium.

In our experiments, the zero-order multifocus traveltime approximation gave consistentely better results than the higher-order approximations. Although a more extensive analysis would have to confirm this observation for more complex media, our experience so far indicates that the zero-order multifocus and the hyperbolic formulas provide the best traveltime approximations.

Additional experiments with a constant velocity gradient have shown similar results, and, hence, have not been included in this paper. In conclusion, outside a certain validity region, where all approximations yield satisfactory results, it cannot be said from our experiments which approximation generally represents the best choice. It seems to us that the choice is strongly model dependent. The actual dependence is still a topic of open research.

Conclusions

We have taken a closer look at the derivations and expressions for the multifocus moveout as elaborated in the last ten years by Gelchinsky and his coworkers and summarized in Gelchinsky et al. (1997). The original derivations were reviewed so as to make them more accessible to a broader audience and to put them into best implementable form. In the process, we obtained a slightly more general multifocus moveout formula that reduces to the original ones when approximations for small source and receiver offsets are taken. We also introduced some modifications in the original asymmetry and multifocus parameters of Gelchinsky with the aim of having the final formulas more amenable to numerical implementation. At this stage, we make no claims the alternative formulas being better approximations than the original ones. An evaluation of which formula is more accurate seems to depend on the model. In our opinion, the present study should contribute to a better understanding of the fundamental as well as geometrically appealling and attractive multifocus idea, which deserves a better recognition in the seismic literature. As a final observation, we mention that a multifocus moveout formula in three-dimensions is still not available. This is a topic of ongoing research.

Acknowledgments

We are grateful for the competent reviews of A. Ehinger, P. Oliva and H. Zien. This research has been funded in part by the National Research Council (CNPq – Brazil), São Paulo State Research Foundation (FAPESP – Brazil) and the sponsors of the WIT Consortium.

References

Červený, V., 1985, The application of ray tracing to the numerical modeling of seismic wavefields in complex structures, *in* Dohr, G., Ed., Seismic shear waves, Part A: Theory, Geophysical Press: Handbook of Geophysical Exploration, Section I: Seismic, **15**, 1–124.

de Bazelaire, E., 1988, Normal moveout revisited: Inhomogeneous media and curved interface: Geophysics, **53**, 143–157.

Gelchinsky, B., 1988, The common-reflecting-element (CRE) method (non-uniform asymmetric multifold system): Ann. Internat. Mtg., ASEG/SEG Intnl. Conf. Exploration Geophysics, 71–75.

Gelchinsky, B., Berkovitch, A., and Keydar, S., 1997. Multifocusing homeomorphic imaging: Parts I and II: Course Notes, Special Course on Homeomorphic Imaging, Seeheim, Germany.

Höcht, G., 1998, Common-reflection-surface stack: Diplomarbeit, Universität Karlsruhe (TH).

Hubral, P., 1983, Computing true amplitude reflections in a laterally inhomogeneous earth: Geophysics, **48**, 1051–1062.

Schleicher, J., Tygel, M., and Hubral, P., 1993, Parabolic and hyperbolic paraxial two-point traveltimes in 3-D media: Geophys. Prosp., **41**, 495–514.

Tygel, M., Müller, Th., Hubral, P., and Schleicher, J., 1997, Eigenwave based multiparameter traveltime expansions: Ann. Internat. Mtg., Soc. Expl. Geophys., Expanded Abstracts, 1770–1773.

Ursin, B., 1982, Quadratic wavefront and traveltime approximations in inhomogeneous layered media with curved interfaces: Geophysics, **47**, 1012–1021.

APPENDIX

Multifocus parameter

Wavefront curvatures

Let us first show how equations (5) follow from standard ray-theoretical arguments. This derivation follows closely the one provided by Gelchinsky et al. (1997) using the basic concepts of ray theory. For the terminology and results to be used below, the reader is referred to Červený (1985).

We start by considering a selected planar ray path in a two-dimensional isotropic model. We assume that the ray is parameterized by the arclength s. Points in the vicinity of this central ray will be described in ray-centered coordinates (s, q), in which q is the transverse coordinate along the ray. The dynamic description of this ray is provided by the scalar quantities $P = P(s)$ and $Q = Q(s)$ computed along the ray, which satisfy the dynamic ray tracing system

$$\frac{d}{ds}\begin{bmatrix} P \\ Q \end{bmatrix} = \begin{bmatrix} 0 & -\frac{v_{qq}}{v} \\ v & 0 \end{bmatrix}\begin{bmatrix} P \\ Q \end{bmatrix} \tag{A-1}$$

Here, $v_{qq} = v_{qq}(s)$ denotes the second derivative of the medium velocity with respect to the transverse coordinate q, evaluated at the point of the ray determined by s. As well known, the quantity $Q = Q(s)$ is the square of the point-source, relative geometrical spreading along the ray.

The central ray under consideration is the zero-offset primary reflection ray introduced in the text (see Figure 1). This ray starts and ends at the central point X_0. For definitness, the (coincident) source and receiver points will be parametrized by $s = 0$ and $s = \ell$, respectively. We have, of course, that $v(0) = v(\ell) = v_0$.

In terms of quantities $P(s)$ and $Q(s)$, the wavefront curvature $K(s)$ along the ray can be expressed by

$$K(s) = v(s)\frac{P(s)}{Q(s)} \, . \tag{A-2}$$

From general properties of linear systems, the general solution of the dynamic ray system (A-1) can be written as a linear combination

$$\begin{bmatrix} P \\ Q \end{bmatrix} = a \begin{bmatrix} P_1 \\ Q_1 \end{bmatrix} + b \begin{bmatrix} P_2 \\ Q_2 \end{bmatrix} , \tag{A-3}$$

of two independent, arbitrarily fixed solutions (P_1, Q_1) and (P_2, Q_2), a and b being constants. Each basic solution pair $(P_i(s), Q_i(s))$ $(i = 1, 2)$ defines an elementary wave that propagates in the vicinity of the central ray (Červený, 1985). It turns out that, within the validity of the paraxial ray theory, any elementary wave that propagates in the vicinity of the central ray and is of the same type as the elementary wave propagating along that ray is described by a solution pair $(P(s), Q(s))$ of the form (A-3). Using equation (A-3) we can rewrite equation (A-2) for the curvature at each point of the ray as

$$K(s) = \frac{q(s)K_1(s) + K_2(s)}{1 + q(s)} , \tag{A-4}$$

where

$$K_i(s) = v(s)\frac{P_i(s)}{Q_i(s)} , \quad i = 1, 2 \quad \text{and} \quad q(s) = \frac{a}{b}\frac{Q_1(s)}{Q_2(s)} . \tag{A-5}$$

Let us now consider the particular *focusing wave* that starts at S with wavefront curvature $K(0) = -K_S$ and emerges at G with wavefront curvature $K(\ell) = K_G$ (see Figure 1). From equation (A-4) we find

$$K_S = -K(0) = -\frac{q(0)K_1(0) + K_2(0)}{1 + q(0)} \tag{A-6}$$

and

$$K_G = K(\ell) = \frac{q(\ell)K_1(\ell) + K_2(\ell)}{1 + q(\ell)} , \tag{A-7}$$

in which

$$q(0) = \frac{a}{b}\frac{Q_1(0)}{Q_2(0)} \quad \text{and} \quad q(\ell) = \frac{a}{b}\frac{Q_1(\ell)}{Q_2(\ell)} . \tag{A-8}$$

As a natural choice for the basic solutions, we select the pairs (P_N, Q_N) and (P_{NIP}, Q_{NIP}) that correspond to the N and NIP *eigenwaves* introduced by Hubral (1983).

These very special elementary waves are characterized by the following two properties:

1. Both waves start and end at the central point X_0, their final wavefronts being coincident with the respective initial ones. Because of the opposite direction of propagation at the initial and endpoints, each eigenwave has curvatures of equal modulus but opposite signs at the coincident source and receiver points;

2. The relative geometrical-spreading factors of the N and NIP waves at the end point X_0 are plus or minus one, respectively.

For a more detailed description and application of the N and NIP eigenwaves, the reader is referred to Hubral (1983). The above-described properties of the N and NIP eigenwaves translate mathematically into the relationships

$$K_N(\ell) = v(\ell)\frac{P_N(\ell)}{Q_N(\ell)} = -\, v(0)\frac{P_N(0)}{Q_N(0)} = -\, K_N(0)\ , \tag{A-9}$$

and

$$\frac{Q_N(\ell)}{Q_N(0)} = 1\ , \tag{A-10}$$

as well as

$$K_{NIP}(\ell) = v(\ell)\frac{P_{NIP}(\ell)}{Q_{NIP}(\ell)} = -\, v(0)\frac{P_{NIP}(0)}{Q_{NIP}(0)} = -\, K_{NIP}(0)\ , \tag{A-11}$$

and

$$\frac{Q_{NIP}(\ell)}{Q_{NIP}(0)} = -1\ . \tag{A-12}$$

In accordance with equations (A-9) and (A-11), we introduce the notations

$$K_N = K_N(\ell) = -K_N(0) \quad \text{and} \quad K_{NIP} = K_{NIP}(\ell) = -K_{NIP}(0)\ . \tag{A-13}$$

In accordance with equations (A-10) and (A-12) inserted into equation (A-8), we also introduce the *modified focusing parameter*,

$$\Gamma = q(\ell) = \frac{a}{b}\frac{Q_N(\ell)}{Q_{NIP}(\ell)} = -\,\frac{a}{b}\frac{Q_N(0)}{Q_{NIP}(0)} = -\, q(0)\ . \tag{A-14}$$

Substituting notations (A-13) and (A-14) into the curvature equations (A-6) and (A-7), we find the following expressions for the source and receiver wavefront curvatures of the focusing wave

$$K_S = -K(0) = \frac{K_{NIP} - \Gamma K_N}{1-\Gamma} \quad \text{and} \quad K_G = K(\ell) = \frac{K_{NIP} + \Gamma K_N}{1+\Gamma}\ . \tag{A-15}$$

The multifocus condition

The condition that an elementary wave traveling in the vicinity of the central ray focuses at a point P along the ray (see Figure 1) can be very simply translated into mathematical terms as the *multifocus condition* (Gelchinsky et al., 1997)

$$\frac{d\sigma_G}{d\sigma_S} = \frac{Q_G}{Q_S}\ . \tag{A-16}$$

Here, $d\sigma_S$ and $d\sigma_G$ are the arc elements of the wavefront at the source and receiver, respectively. The above condition follows from the definition of the dynamical quantity $Q(s)$ as the square of the relative geometrical spreading computed at the point of the ray specified by s for a point source at the focus point P. The consideration of the relative spreadings at the initial and end points of the central ray relative to the same point source at the focusing point P, leads after some simple algebra to equation (A-16). We now observe that the above ratio between the Q variables at source and receiver can be readily computed as

$$\frac{Q_G}{Q_S} \equiv \frac{Q(\ell)}{Q(0)} = \frac{aQ_N(\ell) + bQ_{NIP}(\ell)}{aQ_N(0) + bQ_{NIP}(0)} = \frac{aQ_N + bQ_{NIP}}{aQ_N - bQ_{NIP}} = \frac{\Gamma + 1}{\Gamma - 1} \, . \tag{A-17}$$

As a consequence, the multifocus condition takes the form

$$\frac{d\sigma_G}{d\sigma_S} = \frac{\Gamma + 1}{\Gamma - 1} \, . \tag{A-18}$$

From geometrical considerations in the infinitesimal triangle SX_0S' (see Figure 2), we have the relationship

$$\frac{dx_S}{d\sigma_S} = \frac{1}{\cos\beta_S} \, . \tag{A-19}$$

Substituting this expression and the corresponding equation for $dx_G/d\sigma_G$ into equation (A-18) we obtain

$$\frac{dx_G}{dx_S} = \frac{\Gamma + 1}{\Gamma - 1} \cdot \frac{\cos\beta_S}{\cos\beta_G} \, . \tag{A-20}$$

The above differential equation cannot be solved exactly. Therefore, we will approximate the solution by its Taylor series up to the second-order, i.e.,

$$\Delta x_G = \left.\frac{dx_G}{dx_S}\right|_{x_0} \Delta x_S + \frac{1}{2} \left.\frac{d^2 x_G}{dx_S^2}\right|_{x_0} \Delta x_S^2 \, , \tag{A-21}$$

where he second coefficient can be determined by the derivative of equation (A-20). Thus, we need to determine the derivatives of $\cos\beta_S$ and $\cos\beta_G$ with respect to x_S. Again from Figure 2 we see that

$$\cos\beta_S = \frac{R_S}{L_S} \cos\beta_0 \, , \tag{A-22}$$

where $L_S = \overline{SC_S}$. Therefore, the derivative with respect to x_S is

$$\frac{d}{dx_S}[\cos\beta_S] = -\frac{\cos\beta_S}{L_S} \frac{dL_S}{dx_S} \, . \tag{A-23}$$

Using that

$$\frac{dL_S}{dx_S} = \frac{d\overline{SS'}}{dx_S} = -\sin\beta_S \, , \tag{A-24}$$

we find

$$\frac{d}{dx_S}[\cos\beta_S] = \frac{\sin\beta_S\cos\beta_S}{L_S}\ . \tag{A-25}$$

An analogous equation holds for $d\cos\beta_G/dx_G$. Moreover,

$$\frac{d}{dx_S}[\cos\beta_G] = \frac{d}{dx_G}[\cos\beta_G]\cdot\frac{dx_G}{dx_S} = \frac{\sin\beta_G\cos\beta_S}{L_G}\cdot\frac{\Gamma+1}{\Gamma-1}\ . \tag{A-26}$$

where we have used equation (A-20). The above results readily lead to the relation

$$\frac{d}{dx_S}\left[\frac{\cos\beta_S}{\cos\beta_G}\right] = \frac{\sin\beta_S}{L_S}\cdot\frac{\cos\beta_S}{\cos\beta_G} - \frac{\sin\beta_G}{L_G}\cdot\left(\frac{\cos\beta_S}{\cos\beta_G}\right)^2\cdot\frac{\Gamma+1}{\Gamma-1}\ . \tag{A-27}$$

Computing the above expression on the central ray, i.e., $\beta_S = \beta_G = \beta_0$ as well as $L_S = R_S = 1/K_S$ and $L_G = R_G = 1/K_G$, we obtain

$$\frac{d}{dx_S}\left[\frac{\cos\beta_S}{\cos\beta_G}\right] = \frac{2K_{NIP}\sin\beta_0}{1-\Gamma}\ . \tag{A-28}$$

Hence, in second-order approximation, the solution (A-21) of equation (A-20) reads

$$\Delta x_G = \frac{\Gamma+1}{\Gamma-1}\Delta x_S\left[1+\Delta x_S\frac{K_{NIP}\sin\beta_0}{1-\Gamma}\right]\ . \tag{A-29}$$

This equation describes the relationship between the source and receiver locations of all rays that cut the central ray at the same point P. Since K_{NIP} and β_0 are parameters of the chosen central ray, the relation between Δx_S and Δx_G for a given focus point P is solely determined by the value of Γ.

Conversely, equation (A-29) can be used to determine the value of Γ for any given ray with source at S and receiver at G. Solving equation (A-29) for Γ we find

$$\Gamma = \Gamma_0 + \epsilon\frac{\Delta x_S}{\Delta x_G - \Delta x_S} \tag{A-30}$$

where Γ_0 is given by equation (9) in the text and

$$\epsilon = \sqrt{(1+\alpha\Delta x_S/2)^2 - 2\alpha\Delta x_G} - (1+\alpha\Delta x_S/2)\ . \tag{A-31}$$

Here, α is Gelchinsky's asymmetry paramter, i.e.,

$$\alpha = K_{NIP}\sin\beta_0\ . \tag{A-32}$$

Equation (A-30) is, in fact valid, up to second-order only. Thus, for consistency we have to replace equation (A-31) by its second-order Taylor series. We obtain

$$\epsilon = -\Delta x_G\alpha\left(1+\alpha\frac{\Delta x_G - \Delta x_S}{2}\right) = -\Lambda(1+\Lambda)\frac{2\Delta x_G}{\Delta x_G - \Delta x_S}\ , \tag{A-33}$$

where we have introduced the *modified asymmetry parameter*

$$\Lambda = \alpha \frac{\Delta x_G - \Delta x_S}{2} \, . \tag{A-34}$$

Substituting expression (A-33) into formula (A-30), our final result for the multifocus parameter Γ is equation (8) in the text, namely

$$\Gamma = \Gamma_0 + \frac{\Lambda}{2} \left(1 + \Lambda\right) \left(1 - \Gamma_0^2\right) \, . \tag{A-35}$$

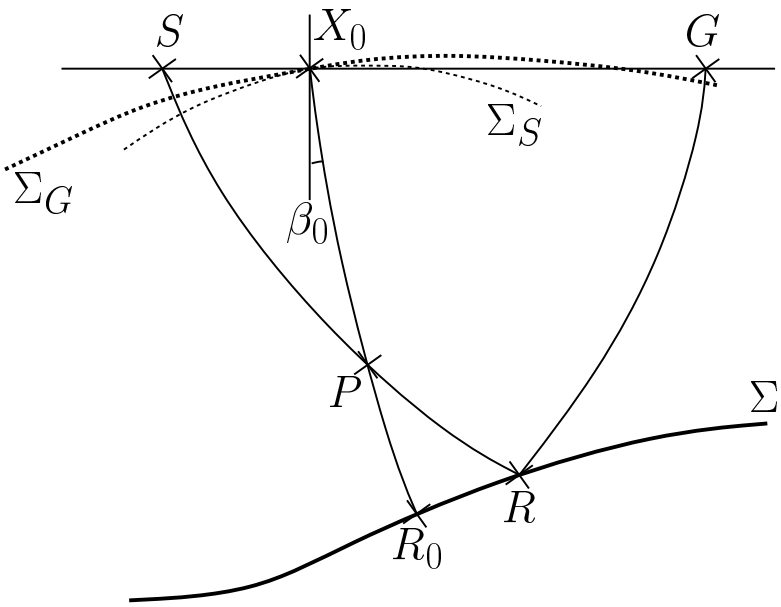

Figure 1: Shown are the central ray $X_0R_0X_0$ and a pair of source and receiver points (S, G) together with its corresponding primary reflected ray SRG, relative to the target reflector Σ. The central ray and the reflection ray focus at point P in depth. Also depicted are two wavefronts of the focusing wave. One, denoted by Σ_S, contains X_0 and has traveled up from P to the source point S. The other, denoted by Σ_G, also contains X_0 and has traveled from P down to the reflector Σ and from there towards the receiver point G. The emergence angle of the central ray is denoted by β_0.

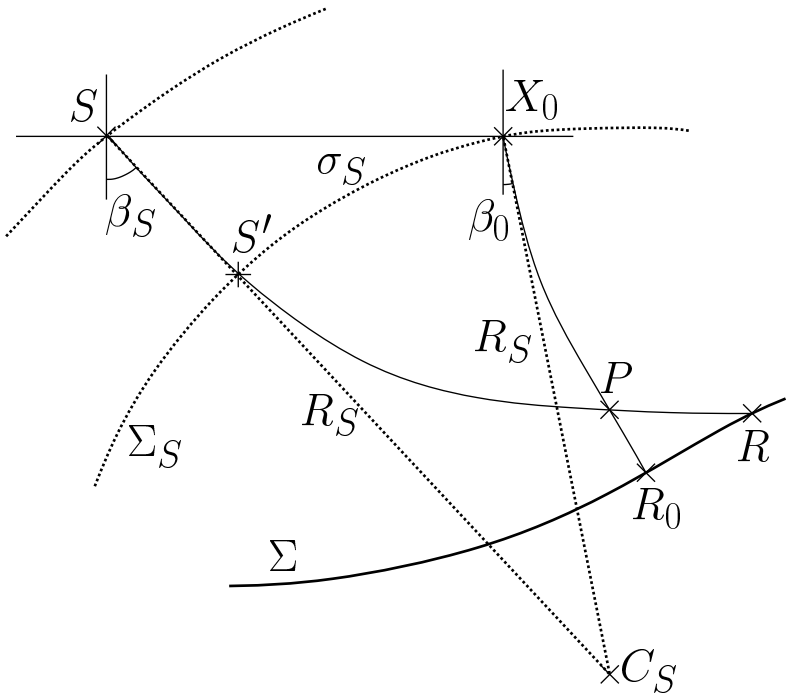

Figure 2: Geometrical construction of multifocus moveout ΔT_S. For details see text.

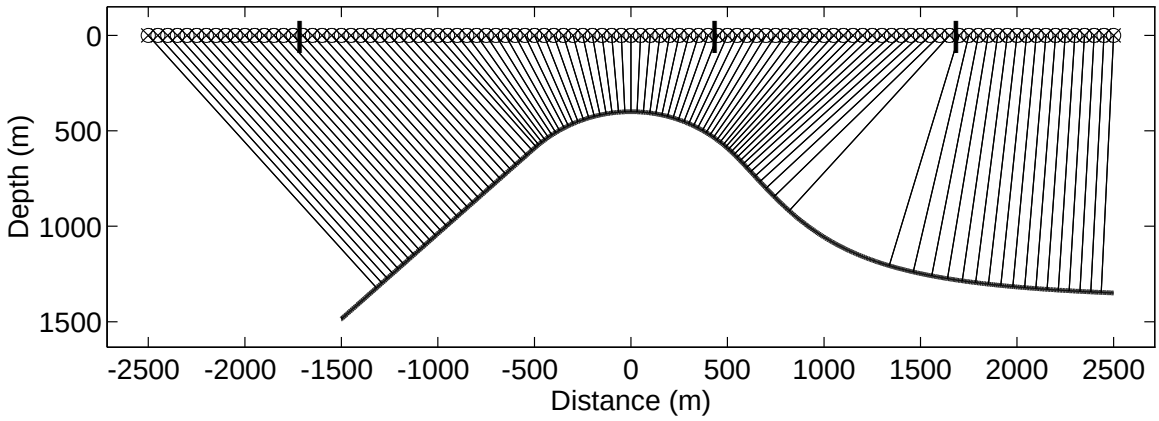

Figure 3: Earth model for the numerical experiment. Indicated are the normal rays and three central points at $X_0 = -1750$ m, 400 m and 1650 m.

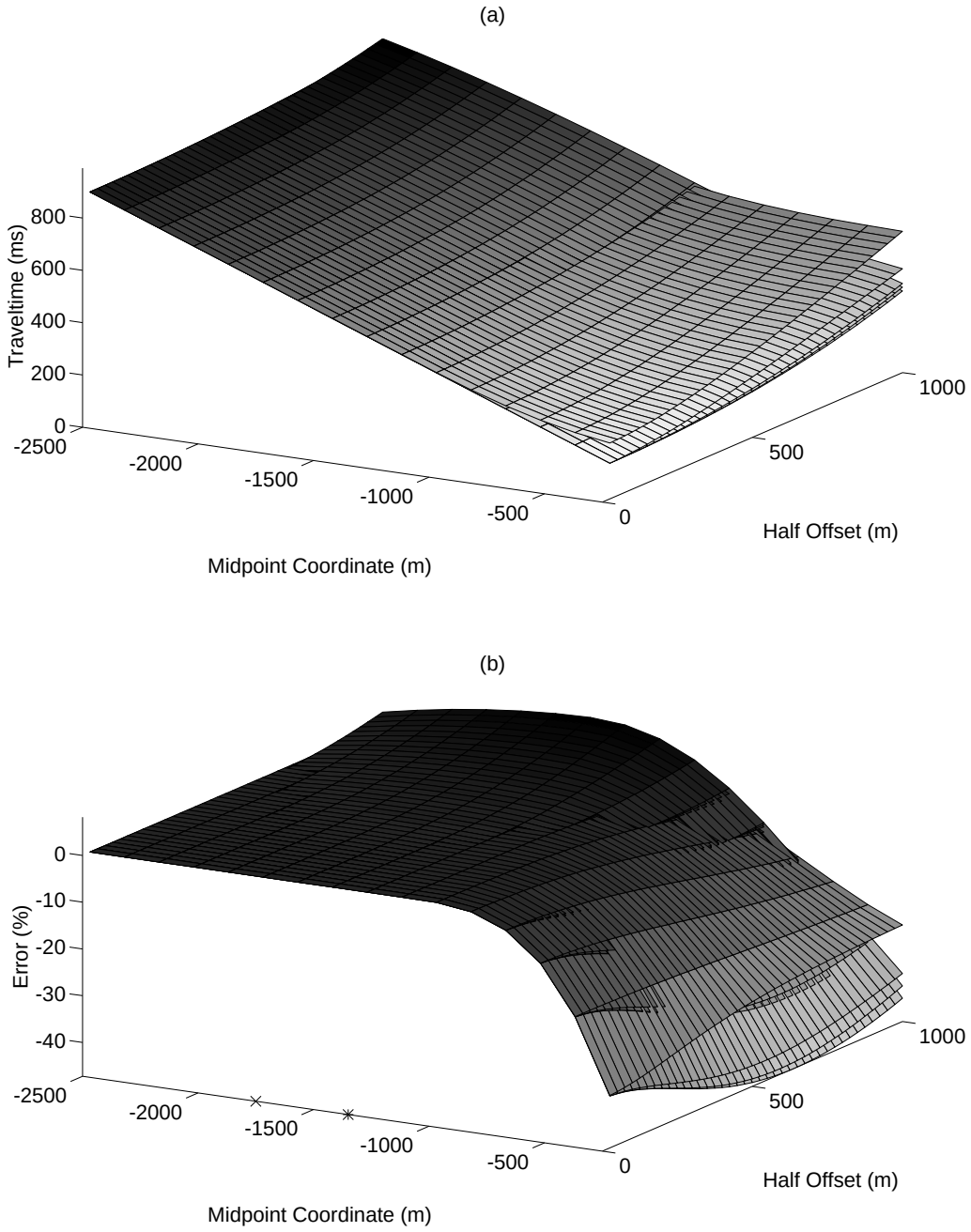

Figure 4: (a) Comparison of approximate and exact traveltime surfaces as functions of midpoint and half-offset. (b) Relative error.

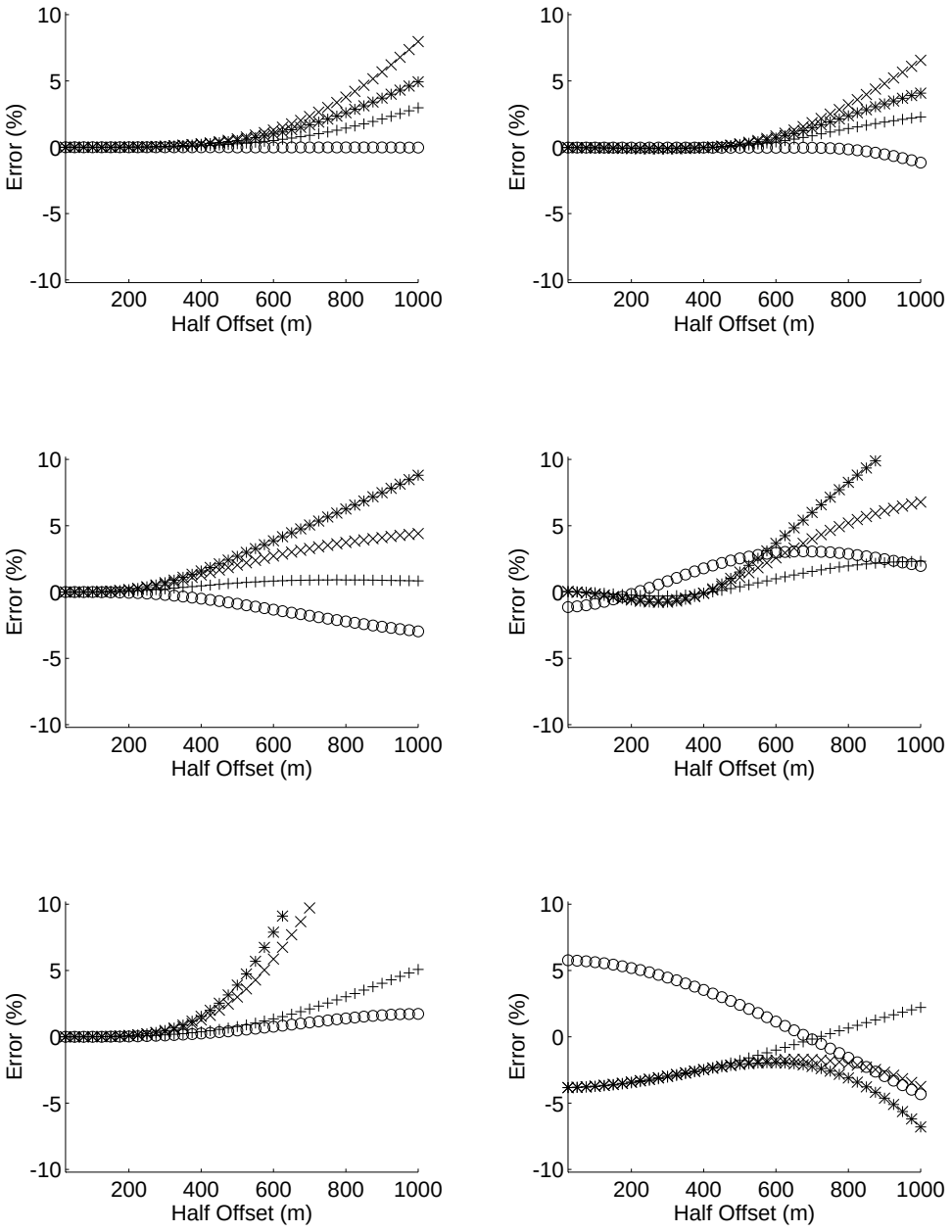

Figure 5: Relative errors of traveltime approximations. Top: Simulation for $X_0 = -1750$ m; left: CMP at X_0, right: CMP at $X_0 + 400$ m. Center: Simulation for $X_0 = 400$ m; left: CMP at X_0, right: CMP at $X_0 + 400$ m. Bottom: Simulation for $X_0 = 1650$ m; left: CMP at X_0, right: CMP at $X_0 + 400$ m.